Andrei Nejur

Structurally Aware Fabrication for Large-Scale, Curved Architectural Skins

Abstract: This paper presents a new construction technique for large complex curved surfaces built from very low thickness sheet materials, reinforced through the structural activation of the dedicated assembly parts. The proposed technique works in several steps. 1) A large architectural curved surface is evaluated using FEA for local buckling and bending under self-weight and the assumption that it will be built from thin sheet material and without an additional structure or reinforcements. 2) The graphical representation of the principal bending moment stress field in the surface is simplified and used as the basis for the generation of a discretization pattern. 3) The discretization pattern is used to generate assembly elements (i. e., flaps) normal to the base surface. 4) The flaps are connected through a system of fins that engage them into a cellular structural system aligned both with the discretization and the stress patterns of the surface. Figure 1 presents a full-scale built prototype demonstrating the workflow.

Fig. 1: General view of the research demonstrator pavilion showcasing the proposed technique. (Image credit Caroline St-Hilaire)

Open Access. © 2023 the authors, published by De Gruyter. BY-NC-ND This work is licensed under the Creative Commons Attribution-NonCommercial-NoDerivatives 4.0 International License.
https://doi.org/10.1515/9783111162683-001

1 Introduction

For large architectural surfaces, discretization and approximation of some kind is usually the only viable way of construction. Regardless of complexity and chosen material, to be constructed, architectural scale surfaces must be divided into pieces or discretized. The segmentation is determined by the limitations of the fabrication process, dimensions and properties of the chosen materials, transport and assembly possibilities (Eigensatz et al. 2010).

1.1 Discretization as a necessity

Discretization is an important method to manage the costs and time required for the construction. It acts as an approximation tool that unlocks the use of cheap planar sheet materials for the construction of complex curved surfaces. However, even if partitioning and approximating architectural curvature and complexity is an effective way of rendering it constructible, it is not a "panacea." In fact, there is a fine line between "just enough" discretization and approximation to make a form feasible for construction and "too much discretization" that wipes off the benefits of manageable dimensions and planarity through unreasonably expensive part multiplication and impossibly long assembly times. Additionally, not all discretizations are built equal. For example, double curvature approximations like PQ meshes (Pottmann 2013) or ruled surface rationalizations (Flöry and Pottmann 2010) are more fabrication friendly due to their planarity and node valence for the former and the simple unfolding on planar sheets for the latter.

1.2 Disadvantages of discretization

Beyond being a necessary step, discretization brings a series of shortcomings to the architectural form. From a structural point of view, the most important is material discontinuity. The discontinuity of the building material induces fault lines in the surface where the pieces are joined together. This can be mitigated using specialized techniques like multilayered surfaces (Fornes 2016; Stanojevic and Takahashi 2019), discrete piece overlaps (Schleicher et al. 2015; La Magna, Schleicher, and Knippers 2016), finger joints (Magna et al. 2013), folds (Demin 2015), and several others. However, with any of those, a comparable material coherence with a single-piece surface is difficult to achieve.

Discretizing a curved architectural surface for fabrication and construction from sheet-based materials requires some sort of approximation. This translates in turn to a deviation from the initial surface that can be simulated in the digital version of the form in the process of design. This deviation is often negligible at the scale of the full

surface and/or is often incorporated in the design intent (Pottmann et al. 2015). The processes that aim to minimize this deviation from the curved base form can reduce the size of discrete parts, thus increasing their number and potentially increasing the costs through assembly complexity. Alternatively parts can be deformed (i. e., by bending or rolling) (Rossi and Nicholas 2018) to make them approximate more closely the subdomain of base surface they represent. They can be deformed in the process of part fabrication (Cai et al. 2012), or they can be a deformed during assembly (Fornes 2016). The latter process combines two steps into one, thus reducing construction time and costs. Deformation during assembly requires additional information to guide the deformation process. Cutting and engraving can encode in some cases this extra information but in others, reference elements (i. e., assembly guides) are required that increase construction complexity and costs.

For flexible and deformable materials that are subjected to structural loads, the simulated and assumed deviation is often accompanied by a deformation due to discretization-induced material discontinuity (Lienhard and Knippers 2013). During conception, this deformation is much harder to predict because it requires high-fidelity (computationally expensive) simulation especially for the joints. During construction, assembly conditions and quality of craftmanship can amplify these uncontrolled deformations leading to undesired structural and aesthetic defects.

Other less desired effects of discretization are the added weight due to the extra connection components, and a limitation of the aesthetic freedom because the architectural image must include, or in other cases take steps to hide, the seams between the discrete parts.

1.3 Self-supporting or supported surfaces

All the above-stated advantages and shortcomings of discretization for large curved architectural surfaces apply in equal measure to self-supported surfaces (i. e., able to carry the self and applied loads) and to surfaces that require a support structure (i. e., a structural network resolving the major load collection and transport to the supports).

Self supported architectural surfaces, beyond inherent material properties (i. e., rigidity or flexibility), rely on folds (Friedman 2016), active bending (Lienhard and Knippers 2015), curvature (Martín-Pastor and García-Alvarado 2019), or multiple layers (Nicholas et al. 2016) to add structural rigidity to the surface. The notable exception here is inflatables that leverage positive internal pressure to gain rigidity (Ayres, Vestartas, and Ramsgaard Thomsen 2018). These methods that add pseudo-thickness to the surface can program surface rigidity through an activation of a specific structural form. The effect of those techniques is still limited by the surface material properties, is local, and implies a certain aesthetic. This aesthetic usually means a constrained proportion between the surface dimensions and the employed curvature radii or fold amplitudes. If the proposed design cannot accommodate such formal constraints, or the structural

demands are greater than the surface material limits, an additional structure is still required.

Supported curved architectural surfaces, even if for the moment we ignore the complexity incurred by an additional structural network (Schling 2018), require a surface-to-structure connection strategy (Schmieder and Mehrtens 2013) that, depending on the rigidity of the chosen material, could imply additional weight, added assembly complexity, and/or increased fabrication costs.

2 Problem statement

Even with all the shortcomings enumerated in the previous section, discretization is the most cost-effective and sometimes the only available solution to construct large-scale architectural curved surfaces from sheet materials. Discretized, self-supported, thin sheet surfaces relying on form for rigidity are well studied and the same can be said about supported surfaces. Contrarily, surfaces that integrate structural reinforcement with the discretization pattern and use the assembly material as support are not covered in the surveyed literature. We can therefore conclude that a gap currently exists in the construction/design techniques used today for large scale structural architectural surfaces built from thin sheet materials. This gap limits the materialization possibilities of self-supported architectural surfaces that do not rely on high curvature and/or local folding for structural reinforcement.

3 Proposed contribution

This paper proposes a new method of construction for architectural-scale curved surfaces from sheet metal, through a unified process of discretization and structural optimization. The proposed technique aims to stand in between methods of construction for self-supported surfaces and methods that rely on a separate structural support for the architectural surface. The technique works by directly deriving the discretization pattern from the structural analysis and then using this pattern together with the material dedicated to discrete piece assembly to reinforce the base surface. Engaging structurally the extra material necessary for joining the discrete parts can improve a) Precision: By using the engaged joints as assembly guides; b) The modulation of the structural properties of the construction independent of the shape of the architectural surface; c) The possibilities to construct smooth and low curvature surfaces without the use of an additional structural system; d) Assembly times, costs and material use compared to architectural surfaces supported by an additional structure.

4 Methodology

The proposed method is the result of research undertaken at University of Montreal's School of Architecture in 2021 (Nejur and Balaban 2022) and was partly developed in a masters research studio in an iterative process between physical prototypes and digital tool development. The method is tested on the construction of a large scale (4.5 m high) thin sheet metal prototype named A(fin)ne. Even though the process presented here is linked to the final prototype, the resulting technique has a much broader application in terms of scale and form. The research and subsequently the method introduced with this paper are presented in several steps: surface pre-processing (Sec. 4.1), structural evaluations (Sec. 4.2), discretization for assembly and structural optimization (Sec. 4.3), assembly geometry generation (Sec. 4.4), fabrication data (Sec. 4.5), and implementation and testing (Sec. 4.6). They are detailed below highlighting the innovations brought to the process.

4.1 Surface pre-processing

The proposed workflow requires the produced architectural surface to be presented as a mesh for discretization but also for structural analysis (i. e., FEA). The chosen discretization technique is a stripification process that decomposes the base mesh into one mesh-face wide ribbons. To facilitate the decomposition and the structural analysis a mesh with constant triangles is required. The triangle meshes with quasi-equal face sizes are appropriate for stripification and FEA as their topology and geometry do not excessively influence the two processes. For our prototype, the base surface was first constructed as a loft then meshed and relaxed as quasi-minimal surface with Kangaroo and it was finally remeshed with an average edge length of 16 cm. This ensured that the average discrete mesh ribbon would end up with an approximate width of 12 cm. Figure 2 shows the first steps in preparing the surface.

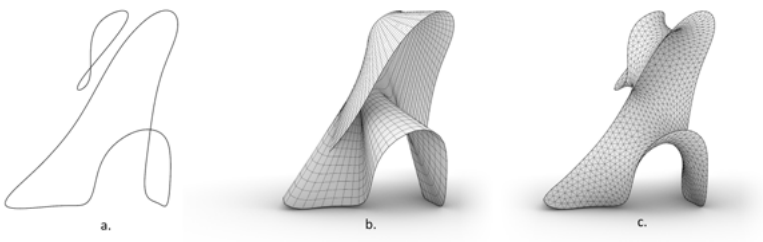

Fig. 2: The form-finding process for the base surface. a) Input curves, b) Meshed loft between curves, c) Relaxed mesh with the soap bubble goal in Kangaroo for Grasshopper. The relaxed mesh is also remeshed with Grasshoppers tri-remesh with a 16 cm average edge.

4.2 Structural evaluation

Next the structural behaviour of the found mesh was tested using the Grasshopper extension Karamba (Preisinger and Heimrath 2014). The mesh was evaluated as an aluminium shell with a constant thickness of 1 mm, rigid supports with no degrees of freedom, and subjected to self-weight. See Fig. 3a for the testing setup. The model exhibited a large deformation mostly caused by the weight of the cantilevering part. The model deformed around an axis defined by a linear area of close to zero Gaussian curvature in the midsection of the surface. Figure 3b shows the simulated deformation of the base mesh based on the self-weight loading scenario as well as the clustering of high bending moment values in the same midsection area. To rigidify the surface, instead of adding curvature in the problem area, we decided to selectively increase the virtual thickness of the metal membrane and thus "program" rigidity into the structure of the pavilion only where it was required.

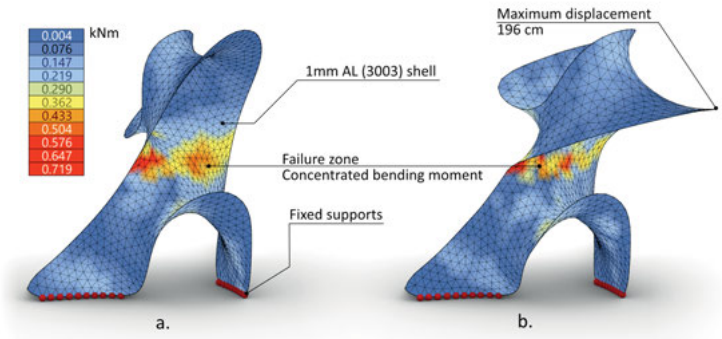

Fig. 3: Karamba simulation of the base mesh under self-weight. The red spheres represent the supports with restricted translations and rotations. a) Un-deformed model, b) Deformed model showing close to 200 cm of displacement.

4.3 Discretization and structural optimization

To increase membrane thickness without the added increase in weight we decided to use the extra material required to assemble the discrete parts of the model (i. e., the assembly tabs). If this extra material can be structurally engaged, it can act as a thicker surface without the added weight. To do this we decided to connect neighbouring tabs with strips of laser-cut metal sheet thus creating a series of "fins" running perpendicular to the surface. Figure 4 shows an early investigative prototype.

Two important issues were identified early in the development process: structural anisotropy and depth. As the rigidity requirement was limited to certain areas and to a certain direction it was clear that not all areas needed the same level of reinforcement

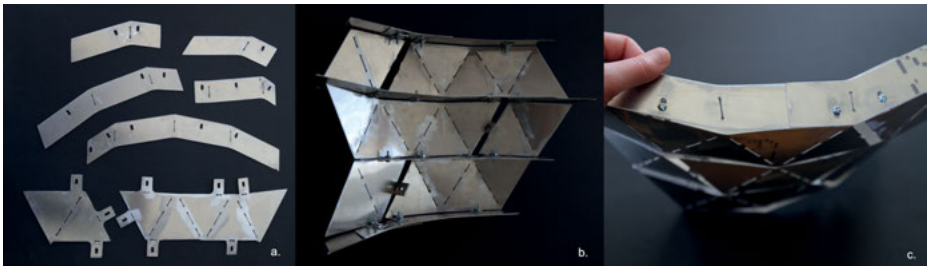

Fig. 4: Early connection prototype. Showing a) Surface pieces and assembly/reinforcement guides (fins), b), c) Fins acting as curvature guides for the assembly.

or "skin depth" and that connections between the tabs had to preferentially follow a certain direction on the surface. As the assembly pattern depends on the discretization of the base mesh into segments, a process for directional-bias stripe segmentation was implemented for the base surface as shown in Fig. 5. Using Karamba, the principal bending moment field was extracted for the curved surface as a network of curves on the base mesh Fig. 5a. After a reduction in complexity the resulting curves shown in Fig. 5b were used to instruct the stripification process (Fig. 5c) for the base mesh using a workflow developed on top of the Ivy add-on for Grasshopper (Nejur and Steinfeld 2016; 2017).

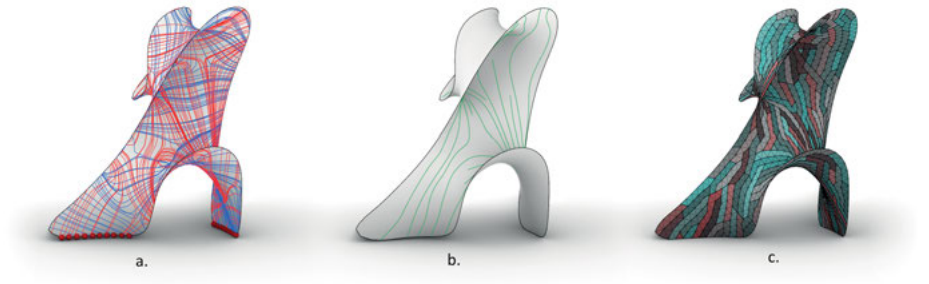

Fig. 5: From FEA simulation to segmentation. a) The graphical representation of the principal bending moments for the aluminum shell under self-weight, b) The simplified bending moment field to be used by the stripification algorithm. c) The resulting segmentation with Ivy Agents.

Using the Ivy API, a series of MeshGraph agents (Nejur 2016) is created on the base mesh. The first agent spawns on a random mesh face and walks on the mesh at each step integrating a mesh face into its subgraph. The agent walks on the dual graph (MeshGraph) of the mesh. In this graph each face of the mesh is a node in the graph and each mesh edge is an edge in the graph. Figure 6 shows the walk of a mesh agent on the base mesh. The MeshGraph representation of the base mesh is not shown to make

the figure more legible. In the agent's subgraph the nodes are named $n_0 \ldots n_{12}$ and the edges $e_0 \ldots e_{11}$. The decision on what mesh face to include in the subgraph at each step is made based on the angle between the next graph edge direction and the tangent direction of the closest simplified bending moment surface curve. In Fig. 6 the direction curves are shown in green as are the tangent vectors $v_0 \ldots v_{11}$ corresponding to each graph edge. The decision mechanism for the next step is shown in the same figure. To walk from n_{11} to the two possible n_{12} variants (red and blue) the algorithm selects the one with the smallest dot product between e_{11} and v_{11} among the red and the blue choices. This ensures that the agent loosely follows the locally closest guide curve and thus the geometry of the principal bending moment network computed by Karamba. The dot product calculation for each edge of the MeshGraph is precomputed for the whole mesh and it is stored as weight (a value between 0 and 1) for each MeshGraph edge. In the end the walk of the agent is simply following the "least weight" choice at every step.

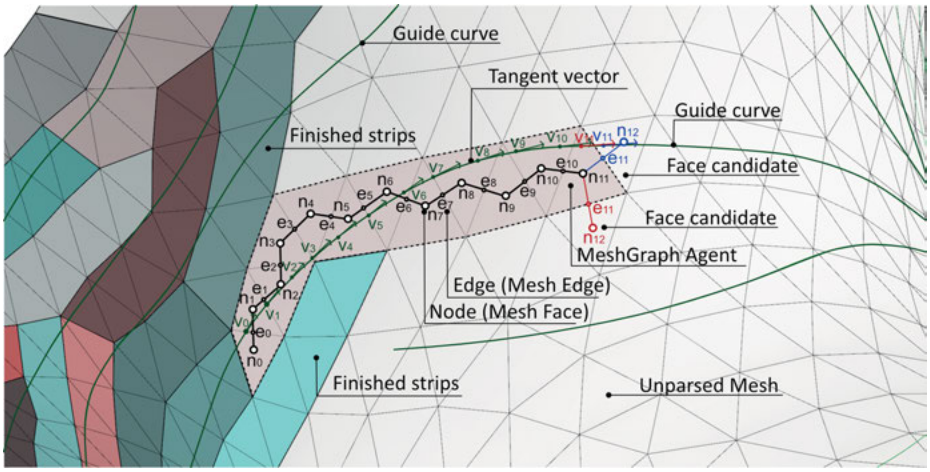

Fig. 6: Detail of the strip growing process. An agent spawns on the base mesh in the vicinity of a recent stripe and walks on the mesh using the local direction (tangent vector) of the nearest guide curve as a reference.

Each agent expires after a preset number of steps (15), thus limiting the maximum number of triangles in a strip. After each agent expiry, a new one is spawned on a node in the immediate vicinity of recently walked nodes (mesh faces). The process continues until all the graph nodes (base mesh faces) are parsed. The shortcoming of this approach is that started strips often run out of mesh faces to parse and result into stubs (strips with fewer than 5 triangles). This happens because the directional field steers the MeshGraph agent into already parsed faces. To overcome this, another algorithm runs in parallel with the stripification process and seeks to unify short strips

end-to-end into larger strips with a maximum length of 25 triangles. Simultaneously strips over 22 triangles long are split approximately in half thus greatly reducing both the stubs and the long strips of faces.

4.4 Secondary structure (the fins)

With the discrete parts of the mesh created, the margins of the strips are used to create a set of fins locally perpendicular to the base mesh and connected to two discrete mesh strips at a time. The creation of the fins happens in several steps. Figure 7 illustrates the process.

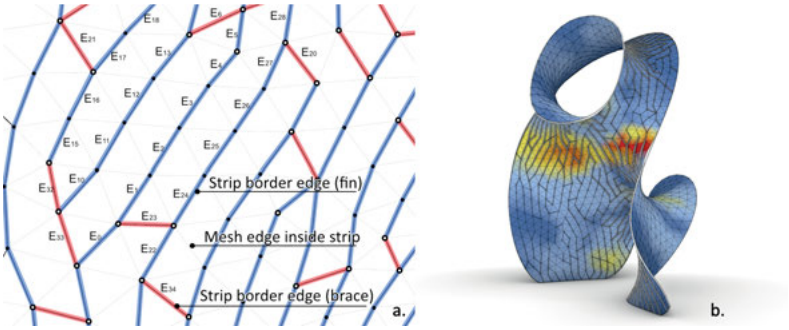

Fig. 7: Secondary structure creation. a) The strip border graph is walked to create the fins and the braces. b) The width of the secondary structure (fins and braces) is controlled by the bending moment values calculated through the FEA analysis.

Step 1 A graph of interconnected strip border edges is created. The new graph contains all the naked edges of the mesh strips with the nodes of the graph being the mesh vertices shared by those edges. The edges of the new graph retain the weight values stored in the corresponding MeshGraph edges used previously to produce the strips.

Step 2 The new graph is "walked" with a preference for the highest weight edges (shown in blue in Fig. 7a) and a constraint of walking on edges with no more than 30 degrees between their walk-oriented directions. This is to avoid large fin deformations during fabrication due to bending. In Fig. 7a mesh edges E0, E1, E2, E3, E4 are part of the same walk that will become a continuous fin. E4 and E5 are split due to the angle deviation. The length of the walks is limited to 10 consecutive edges to facilitate fabrication and assembly. The process produces a series of unconnected edges that will remain singletons (braces) between the fins. They are shown in red in Fig. 7a.

Step 3 The resulting polylines are extruded in the normal direction of each contained mesh vertex. The amount of the extrusion at each vertex is based on the vertex flexion

value averaged from the faces touching the vertex. The averaged values are remapped into usable millimeter values (25–50 mm) for the extrusion process. Figure 7b shows the correlation between fin height and bending moment.

With the secondary structure in place and fused to the base mesh a new structural simulation with Karamba reveals that the maximum deformation has been reduced from 1960 mm to just 2 mm.

4.5 Fabrication data

For fabrication, the discreet parts of the prototype (i. e., strips and fins) were unfolded flat and tagged using Ivy. To enable manual assembly the strips were clustered in 10 sectors each not exceeding 2 m × 2 m and max 20 kg. The clustering was done using Ivy's k-means algorithm implementation to produce 10 compact groups of mesh faces. The strip clusters are created through the allocation of each strip to the cluster where the largest number of its faces reside. Figure 10 shows the result of the clustering process.

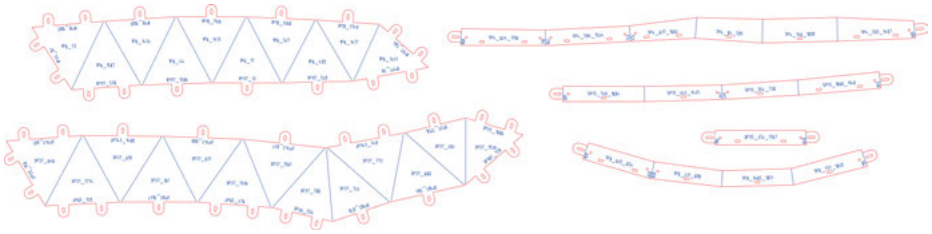

Fig. 8: The 2D fabrication data produced by the script. Left: several typical strips with connection tabs and assembly tags to be cut from 1 mm aluminium sheet. Right: Typical fins and a brace with longitudinal tabs for continuity and oblong holes for the connections to the strip tabs. The fins are cut from 1.5 mm aluminium sheet.

The unfolded strips are tagged using the standard Ivy workflow (Nejur 2016). Each mesh strip receives text tags in all face centers and next to the border edges. Each tag encodes the sector, strip, and face number. The center tag numbers refer to the current face and strip while the border tags identify the connecting ones. Each strip naked edge is fitted with a connection tab with strip end edges receiving two tabs for added stiffness in the higher strain areas and a reduced assembly complexity. To accommodate the nut and bolt manual assembly strategy the tabs are fitted with oblong holes. To accommodate the curvature radius of the bent 1 mm thick tabs each unfolded stripe contour is offset inwards with 1.5 mm.

The perpendicular fins are constructed as individual pieces from the extruded polylines presented in Sec. 4.4. The fins use the strip tabs to connect to the base surface and are

intercalated between each pair of strip tabs. To connect to the tabs, the fin geometry includes oblong holes corresponding to each tab hole. To match fins with the relevant strips and tabs each fin segment is tagged with the number of the adjacent mesh faces also present on the strips. Fins are fitted with end tabs to ensure the structural continuity of the fin network.

4.6 Implementation and testing

The workflow was tuned and tested during a research studio at University of Montreal School of Architecture. Because the ambition was to build the large-scale demonstrator by hand, the physical prototype to digital development approach was useful in tuning the scale of the final build towards something buildable by non-specialists. The final full-scale prototype called A(fin)ne was built in September 2021 over the course of 5 days by 12 students and two tutors with hand tools only. The final prototype stood 4.5 m tall, had 202 laser-cut stripes, 465 fins and braces, approximately 3200 bolts and a surface area of 16.7 m^2. The prototype remained on display for 3 months inside the faculty building.

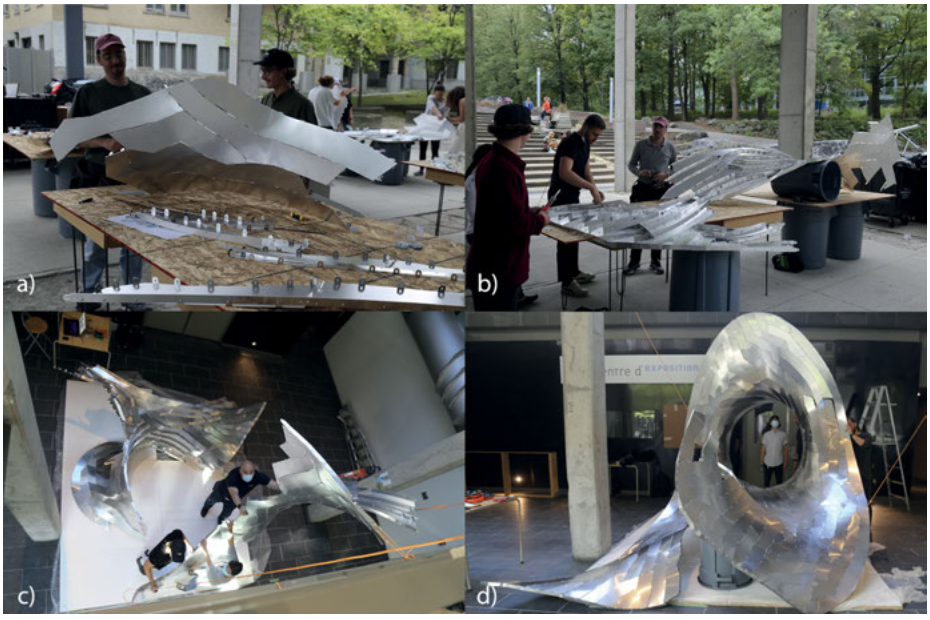

Fig. 9: The assembly process lasted 5 days. First the cut strips were pre-processed a) and assembled into sectors b) that were brought together in the full prototype c) and d). (Image credit Caroline St-Hilaire)

5 Discussion, limitations, and future work

The proposed method while very effective at reinforcing the 1 mm aluminum shell for the proposed scope, also induces fabrication and assembly problems and its use revealed a series of limitations during construction. For instance, it was difficult to manage the large-scale assembly of the sectors, due to their limited rigidity and their weight-induced deformations coupled with the interlocking, finger-like geometry shown in Fig. 10. Suspending the individual sectors and assembling them in mid-air was the only way to overcome the hurdle. The programed structural anisotropy did not account enough for lateral efforts. If pushed firmly the built prototype would sway and vibrate and had to be attached to a walkway for safety. To address this, future iterations of the method will include more complex bracing. Other considered avenues of investigation are multilayer structures. Through the inclusion of additional partial layers of strips on the back (fin) side of the surface, a more controlled aesthetic for both sides of the surface and an improved rigidity will be possible.

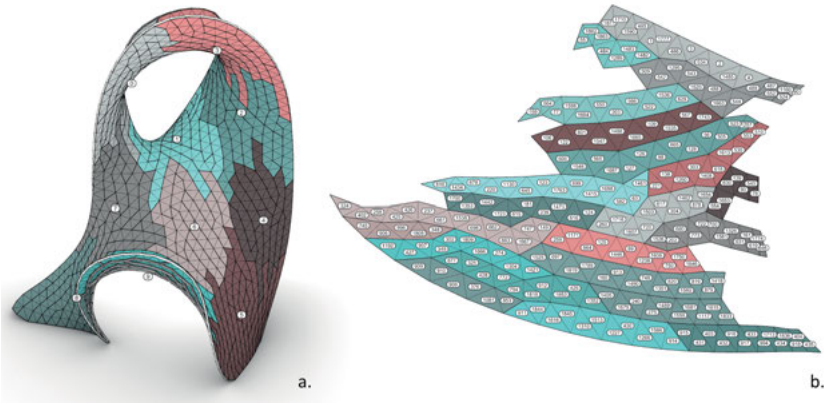

Fig. 10: The geometry of the sectors was designed to hide the seams and avoid folding due to faulty assembly. However, the sector fingers were a lot harder to match than anticipated during the actual construction process. a) A general view of the sector distribution. b) Detail view of sector 3 showing mesh face numbers used for assembly refence.

6 Conclusion

In this paper we have shown, a new method for building self-supported, large, curved, architectural surfaces from ultra-low thickness metal sheet using the segmentation of the surface for fabrication and engaging the dedicated assembly material for structural rigidity. Beyond augmented structural stiffness, the method we proposed improves

assembly times and assembly precision especially for low-tech, low budget construction scenarios. Our method significantly reduces weight compared to surfaces supported by a dedicated structure and unlocks an interesting aesthetic for large curved architectural surfaces. The method we proposed successfully addresses an existing gap in the existing research of large, curved, self-supported architectural surfaces, built from sheet metal, that cannot rely on curvature or folds for rigidity.

The initial base surface (without the fins) weighed an estimated 55 kg including the bolts and the connection tabs and displayed a simulated 1960 mm deformation. The proposed thick skin including the fins, bolts and the connection tabs weighed an estimated 80 kg and displayed a deformation of only 2 mm similar to a supported surface but with a fraction of the weight and associated costs.

Acknowledgement

The author of the paper acknowledges as co-authors of the built pavilion, the team of students and tutors of the ARC 6801H 2021 research studio. They are as follows. Students: Alphonso Francis, Belanger Nicolas, Berube Camille, Faltas Youstina, Gamachio Eva, Langelier Marc-Antoine, Larouche-Wilson Kevin, Mansy Mariam, Mireault Pierre-Alexandre, Morissette Olivier, Nahra Ellie, Poulin Delphie, St-Hillaire Caroline; Tutors: Thomas Balaban and Andrei Nejur. The author also acknowledges the support offered for the building of the pavilion by the School of Architecture at University of Montreal, Aluquebec, and Industries B37.

References

Ayres, P., P. Vestartas, and M. Ramsgaard Thomsen. 2018. Enlisting clustering and graph-traversal methods for cutting pattern and net topology design in pneumatic hybrids. In *Humanizing Digital Reality: Design Modelling Symposium Paris 2017,* 285–94. Springer.

Cai, Z.-Y., Y.-W. Lan, M.-Z. Li, Z.-Q. Hu, and M. Wang. 2012. Continuous sheet metal forming for doubly curved surface parts. *International Journal of Precision Engineering and Manufacturing* 13: 1997–2003.

Demin, D. 2015. The rose pavilion. In *Proceedings of IASS Annual Symposia,* 2015:1–9. International Association for Shell and Spatial Structures (IASS).

Eigensatz, M., M. Deuss, Al. Schiftner, M. Kilian, N. J. Mitra, H. Pottmann, and M. Pauly. 2010. Case studies in cost-optimized paneling of architectural freeform surfaces. *Advances in Architectural Geometry* 2010: 49–72.

Flöry, S., and H. Pottmann. 2010. Ruled surfaces for rationalization and design in architecture.

Fornes, M. 2016. The art of the prototypical. *Architectural Design* 86 (2): 60–67.

Friedman, T. 2016. Foldfinding – a novel approach to the design and fabrication of folded structures. In *Proceedings of IASS Annual Symposia,* 2016:1–10. International Association for Shell and Spatial Structures (IASS).

La Magna, R., M. Gabler, S. Reichert, T. Schwinn, F. Waimer, A. Menges, and J. Knippers. 2013. From nature to fabrication: Biomimetic design principles for the production of complex spatial structures. *International Journal of Space Structures* 28 (1): 27–39.

La Magna, R., S. Schleicher, and J. Knippers. 2016. Bending-active plates. *Advances in Architectural Geometry* 2016: 170–87.

Lienhard, J., and J. Knippers. 2013. Considerations on the scaling of bending-active structures. *International Journal of Space Structures* 28 (3-4): 137–48.

Lienhard, J., and J. Knippers. 2015. Bending-active structures. *Bautechnik* 92 (6): 394–402. DOI: 10.1002/bate.201500007

Martín-Pastor, A., and R. García-Alvarado. 2019. Developable wooden surfaces for lightweight architecture: bio-dune pavilion. *Digital Wood Design: Innovative Techniques of Representation in Architectural Design,* 1481–1500.

Nejur, A. 2016. Ivy for Grasshopper Manual: Version 0.802. *Digital Design Research Repository Andrei Nejur.*

Nejur, A., and T. Balaban. 2022. The A(Fin)Ne pavilion. In *Co-Creating the Future: Inclusion in and through Design. Proceedings of the 40th Conference on Education and Research in Computer Aided Architectural Design in Europe* (ECAADe 2022), 2:507–16.

Nejur, A., and K. Steinfeld. 2016. Ivy bringing a weighted-mesh representation to bear on generative architectural design applications. In *ACADIA* 2016, 140–51. Ann Arbor MI: CUMINCAD.

Nejur, A., and K. Steinfeld. 2017. Ivy: Progress in developing practical applications for a weighted-mesh representation for use in generative architectural design. In *ACADIA* 2017, 446–55. Boston, MA: CUMINCAD.

Nicholas, P., D. Stasiuk, E. Nørgaard, C. Hutchinson, and M. Ramsgaard Thomsen. 2016. An integrated modelling and toolpathing approach for a frameless stressed skin structure, fabricated using robotic incremental sheet forming. *Robotic Fabrication in Architecture, Art and Design* 2016, 62–77.

Pottmann, H. 2013. Architectural geometry and fabrication-aware design. *Nexus Network Journal,* 15 (2): 195–208.

Pottmann, H., M. Eigensatz, A. Vaxman, and J. Wallner. 2015. Architectural geometry. *Computers & Graphics* 47: 145–64.

Preisinger, C., and M. Heimrath. 2014. Karamba — a toolkit for parametric structural design. *Structural Engineering International* 24 (2): 217–21.

Rossi, G., and P. Nicholas. 2018. Modelling a complex fabrication system: New design tools for Doubly curved metal surfaces fabricated using the english wheel. In *Proceedings of ECAADe 2018: Computing for a Better Tomorrow,* 811–20.

Schleicher, S., A. Rastetter, R. La Magna, A. Schönbrunner, N. Haberbosch, and J. Knippers. 2015. Form-finding and design potentials of bending-active plate structures. In *Modelling Behaviour,* 53–63. Springer.

Schling, E. 2018. Design and construction of curved support structures with repetitive parameters. In *Advances in Architectural Geometry* 2018.

Schmieder, M., and P. Mehrtens. 2013. Cladding freeform surfaces with curved metal panels — a complete digital production chain. *In Advances in Architectural Geometry* 2012, Eds. L. Hesselgren, S. Sharma, J. Wallner, N. Baldassini, P. Bompas, and J. Raynaud, 237–42. Vienna: Springer Vienna.

Stanojevic, D., and K. Takahashi. 2019. Strip-based double-layered lightweight timber structure. *Proceedings of IASS Annual Symposia* 2019 (11): 1–8.